PHYSICAL REVIEW B **82**, 041402(R) (2010)

Phonon switching and combined Fano-Rice effect in optical spectra of bilayer graphene

E. Cappelluti,[1,2] L. Benfatto,[1,2] and A. B. Kuzmenko[3]
[1]*Istituto dei Sistemi Complessi, sezione Sapienza, CNR, via dei Taurini 19, 00185 Rome, Italy*
[2]*Dipartimento di Fisica, Università "La Sapienza," P.le A. Moro 2, 00185 Rome, Italy*
[3]*DPMC, Université de Genève, 1211 Genève, Switzerland*
(Received 16 June 2010; published 9 July 2010)

Recent infrared measurements of phonon peaks in gated bilayer graphene reveal two striking signatures of electron-phonon interaction: an asymmetric Fano lineshape and a giant variation in the peak intensity as a function of the applied gate voltage. In this Rapid Communication we provide a unified theoretical framework which accounts for both these effects and unveils the occurrence of a switching mechanism between symmetric (E_g) and antisymmetric (E_u) phonon modes as dominant channel in the optical response. A complete phase diagram of the optical phonon response is also presented, as a function of both the charge density and the band gap.

DOI: 10.1103/PhysRevB.82.041402 PACS number(s): 78.67.Wj, 63.22.Rc, 78.30.−j

Single and multilayer graphenes are among the most promising systems for the development of carbon-based devices in electronics. Bilayer graphene is of particular interest because a controlled tunable gap in the electronic spectrum can be there induced by applying one (or more) external gate voltages,[1–3] as observed by transport[3] and optical measurements.[4–7] The potential interest in application has triggered also an intense research on the vibrational properties, that can be used, for instance, for a careful characterization of the number of layers, the charge doping, and the amount of disorder.[8–10] Large part of the work in this context has focused on the properties of the in-plane E_g mode at $\omega \approx 0.2$ eV which is present in single as well as in bilayer systems, and which can be probed by Raman spectroscopy.[9–14]

Recently, phonon peaks in the energy range $\omega \approx 0.2$ eV have been reported also in infrared (IR) optical measurements of bilayer graphene,[15,16] showing a rather different phenomenology with respect to Raman spectroscopy. In particular, the observed IR phonon peak presents a strong dependence of the intensity and of the Fano-type asymmetry as a function of the applied gate voltage.[15,16] These features have been attributed, respectively, to a charged phonon effect for the E_u antisymmetric (A) mode,[15] or, at $n=0$, to the emergence of a Fano profile for the E_g symmetric (S) mode, whose optical activity can be triggered by the electrostatic potential difference Δ between the two carbon planes.[16] However, the possible connection between these two alternative views is still unclear.

In this Rapid Communication we provide a unified microscopic framework that allows us to elucidate the relative role of E_u and E_g phonon modes in bilayer graphene with regards to the infrared activity and the Fano asymmetry of the observed phonon peaks. We present a complete phase diagram for the strength of the phonon modes and their Fano properties as functions of the chemical potential and Δ, showing that a switching mechanism between the dominance of E_u or E_g mode can be controlled by the external gate voltage. Our work permits thus reconciling within a unique approach the phonon-peak features observed by different experimental groups.[15,16]

To compute the conductivity of bilayer graphene we work in the 4×4 basis of the atomic orbitals $\Psi_{\mathbf{k}}^{\dagger}=(a_{1\mathbf{k}}^{\dagger},b_{1\mathbf{k}}^{\dagger},a_{2\mathbf{k}}^{\dagger},b_{2\mathbf{k}}^{\dagger})$, where $a_{i\mathbf{k}}^{\dagger}$ and $b_{i\mathbf{k}}^{\dagger}$ operators create an electron in the layer i and on the sublattice A or B, respectively. In this basis, the Hamiltonian for bilayer graphene near the K point reads:[17] $\hat{H}_{\mathbf{k}}=\{\hbar v\mathbf{k}\cdot\hat{I}(\hat{\boldsymbol{\sigma}})+(\Delta/2)\hat{\sigma}_z(\hat{I})+(\gamma/2)[\hat{\sigma}_x(\hat{\sigma}_x)+\hat{\sigma}_y(\hat{\sigma}_y)]\}$, where $\hat{\sigma}_i$ and $\hat{I}$ are 2×2 Pauli matrices and the unit matrix, respectively, and $\hat{A}(\hat{B})\equiv\hat{A}\otimes\hat{B}$. Here v is the Fermi velocity for single-layer graphene and γ is the interlayer hopping. The electrostatic potential difference Δ induces a gap in the diagonalized bands $\epsilon_{\mathbf{k},n}$ (Ref. 1), labeled according to Fig. 1(a).

We set the electric field of the infrared radiation along the x axis, so that the electric current reads $j=\Sigma_{\mathbf{k}}\Psi_{\mathbf{k}}^{\dagger}\hat{j}_{\mathbf{k}}\Psi_{\mathbf{k}}$, where $\hat{j}_{\mathbf{k}}=-ev\hat{I}(\hat{\sigma}_x)$. The two E_u and E_g in-plane optical phonons have degenerate longitudinal and transverse polarization at zero momentum $\mathbf{q}=0$.[17] We can write the electron-phonon interaction for these modes as: $H_{\mathrm{ep}}=\Sigma_{\nu}V_{\nu}\phi_{\nu}$, where ϕ_{ν} is the dimensionless lattice displacement for the $\nu=\mathrm{A},\mathrm{S}$ branch at $\mathbf{q}=0$, $V_{\nu}=\Sigma_{\mathbf{k}},\Psi_{\mathbf{k}}^{\dagger}\hat{V}_{\nu}\Psi_{\mathbf{k}}$ is the corresponding electron-phonon scattering operator. For a choice of the longitudinal polarization along x, one finds $\hat{V}_{\mathrm{A}}=ig\hat{\sigma}_z(\hat{\sigma}_y)$ and $\hat{V}_{\mathrm{S}}=ig\hat{I}(\hat{\sigma}_y)$ (Ref. 17), where g is the electron-phonon coupling.

Let us consider first the case of ungapped bilayer graphene ($\Delta=0$), where only the A mode is optically active. Since graphene is a nonpolar system, the bare dipole induced by the rigid shift of the valence charges upon the A lattice distortion is extremely small.[15] Nevertheless, an optical pho-

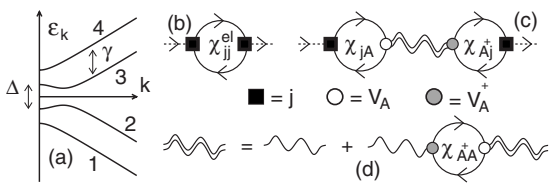

FIG. 1. (a) Scheme of the band structure. (b)–(d) Relevant diagrams entering the optical conductivity for $\Delta=0$: dashed, solid, and wavy lines represent the photon, the electron, and the phonon Green's functions, respectively. Squares and circles are the current and the electron-phonon-scattering matrices $\hat{j}$, $\hat{V}_{\mathrm{A}}$, $\hat{V}_{\mathrm{A}}^{\dagger}$, respectively.

non response can be still mediated by the conduction charges in the presence of the electron-phonon interaction, as suggested by Rice[18] in the context of organic and fullerene compounds. The total optical conductivity of the system is computed as $\sigma(\omega)=-\chi_{jj}(\omega)/i\omega$, where $\chi_{jj}(\omega)=-\langle jj\rangle_\omega$ is the current-current response function. In the presence of electron-phonon interaction, one can identify two classes of contributions in $\chi_{jj}(\omega)$, namely, $\chi_{jj}(\omega)=\chi_{jj}^{\rm el}(\omega)+\chi_{jj}^{\rm ep}(\omega)$. The former, depicted in Fig. 1(b), describes electronic excitations (see, for example, Ref. 19) while the latter contains all the diagrams which can be split in two by cutting one phonon propagator [Fig. 1(c)].[18] We can write thus

$$\chi_{jj}^{\rm ep}(\omega)=\chi_{j\rm A}(\omega)D_{\rm AA}(\omega)\chi_{\rm A^\dagger j}(\omega), \tag{1}$$

where $\chi_{j\rm A}(\omega)=-\langle jV_{\rm A}\rangle_\omega$, $\chi_{\rm A^\dagger j}(\omega)=-\langle V_{\rm A}^\dagger j\rangle_\omega$ are the mixed current-phonon response functions and $D_{\rm AA}(\omega)=-\langle\phi_{\rm A}\phi_{\rm A}\rangle_\omega \approx[\omega-\omega_{\rm A}+i\Gamma_{\rm A}/2]^{-1}$ is the phonon propagator with frequency $\omega_{\rm A}$ and linewidth $\Gamma_{\rm A}$ renormalized by the phonon self-energy $\chi_{\rm A^\dagger A}$ [Fig. 1(d)]. It should be emphasized that two *different* response functions, $\chi_{jj}^{\rm el}$ and $\chi_{j\rm A}$, enter in the above decomposition of $\sigma(\omega)$. This distinction, that has been neglected in the original formulation,[18] is, however, crucial, because it implies that the allowed particle-hole excitations of the system will contribute in a different way to the electronic optical background, related to $\chi_{jj}^{\rm el}$, to the phonon renormalization, controlled by $\chi_{\rm A^\dagger A}$, or to the electron-phonon optical response, controlled by $\chi_{j\rm A}$.

Equation (1) leads to the onset, in the real part of the optical conductivity $\sigma'_{\rm ep}(\omega)=-{\rm Im}\,\chi_{jj}^{\rm ep}(\omega)/\omega$, of a phonon peak at $\omega_{\rm A}$. Indeed, using the relation $\chi_{\rm A^\dagger j}(\omega)=\chi_{j\rm A}(\omega)$ and taking real and imaginary parts of each element in Eq. (1), we get

$$\sigma'_{\rm ep}(\omega)_{\omega\approx\omega_{\rm A}}\approx\frac{2[\chi'_{j\rm A}(\omega_{\rm A})]^2}{\omega_{\rm A}\Gamma_{\rm A}}\left[\frac{q_{\rm A}^2-1+2q_{\rm A}z}{q_{\rm A}^2(1+z^2)}\right], \tag{2}$$

where $z=2[\omega-\omega_{\rm A}]/\Gamma_{\rm A}$ and where

$$q_{\rm A}=-\frac{\chi'_{j\rm A}(\omega_{\rm A})}{\chi''_{j\rm A}(\omega_{\rm A})}. \tag{3}$$

Equation (2) has exactly the same structure as the Fano formula.[20] The derivation of Eqs. (2) and (3) shows not only that in bilayer graphene the Fano effect originates from a correct implementation of the charged-phonon Rice theory but it also provides a compelling procedure to evaluate on microscopic grounds the shape and the intensity of the phonon peak. For instance, from Eqs. (2) and (3) we can identify the ω-integrated peak area as $W'_{\rm A}=\pi[\chi'^2_{j\rm A}(\omega_{\rm A})-\chi''^2_{j\rm A}(\omega_{\rm A})]/\omega_{\rm A}=(1-1/q_{\rm A}^2)[\pi\chi'^2_{j\rm A}(\omega_{\rm A})/\omega_{\rm A}]$. Since the sign of $W'_{\rm A}$ depends on $q_{\rm A}$ it can be convenient, as done in Ref. 15, to define a "bare" intensity as $W_{\rm A}=\pi\chi'^2_{j\rm A}(\omega_{\rm A})/\omega_{\rm A}$, which coincides with $W'_{\rm A}$ in the limit $|q_{\rm A}|\to\infty$, when Eq. (2) reduces to a conventional Lorentzian peak with weight $W_{\rm A}$. Note, however, that in the opposite case $|q_{\rm A}|\approx 0$ one recovers from Eqs. (2) and (3) a completely *negative* Lorentzian peak, of intensity $-\pi|\chi''_{j\rm A}(\omega_{\rm A})|^2/\omega_{\rm A}$, so that the definition of "intensity" of the phonon peak can be ambiguous in the presence of the Fano effect. A more convenient quantity to parameterize the strength of the phonon peak is $p_{\rm A}=\pi|\chi_{j\rm A}(\omega_{\rm A})|^2/\omega_{\rm A}$

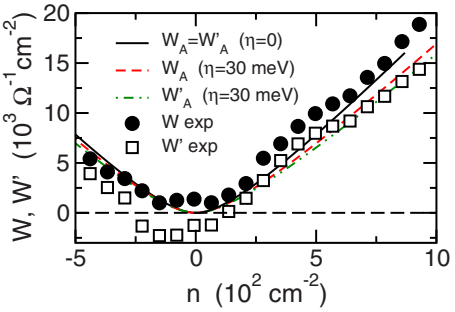

FIG. 2. (Color online) $W_{\rm A}$, $W'_{\rm A}$ intensities of the E_u mode as a function of the charge concentration n for $\Delta=0$ and $\eta=0$ and 30 meV. Also shown are experimental data from Ref. 15 for the bare intensity $W_{\rm exp}$ and the ω-integrated one $W'_{\rm exp}$.

$=W_{\rm A}(1+1/q_{\rm A}^2)$, which is always positive and vanishes when the phonon peak is completely absent.

Equations (2) and (3) can be computed analytically by using the noninteracting electron Green's functions. The quantity $\chi_{j\rm A}$ has the typical structure of a particle-hole Lindhard response function with proper coherence factors $C_{j\rm A}^{nm}$ weighting the contributions of the various excitations between n and m bands. In particular, using the explicit matrix expressions of $\hat{j}$ and $\hat{V}_{\rm A}$ operators, one gets

$$\chi_{j\rm A}(\omega)=\chi_{j\rm A}^{12}(\omega)+\chi_{j\rm A}^{13}(\omega)-\chi_{j\rm A}^{24}(\omega)-\chi_{j\rm A}^{34}(\omega), \tag{4}$$

where $\chi_{j\rm A}^{nm}(\omega)=\pi_{j\rm A}^{nm}(\omega)-\pi_{j\rm A}^{mn}(\omega)$ and

$$\pi_{j\rm A}^{nm}(\omega)=\sum_{\mathbf{k}}C_{j{\rm A},\mathbf{k}}^{nm}\frac{f(\epsilon_{\mathbf{k},n}-\mu)-f(\epsilon_{\mathbf{k},m}-\mu)}{\epsilon_{\mathbf{k},n}-\epsilon_{\mathbf{k},m}+\hbar\omega+i\eta}. \tag{5}$$

Here $f(x)=1/[\exp(x/T)+1]$ is the Fermi function, $C_{j{\rm A},\mathbf{k}}^{nm}=(gev N_s N_v)\gamma/4\sqrt{(\hbar v k)^2+\gamma^2}$ for n,m as in Eq. (4), and zero otherwise, μ is the chemical potential, $N_s=N_v=2$ are the spin and valley degeneracies, and the η factor takes into account broadening effects due to impurities and inhomogeneities. In the clean limit, $\eta=0$, we obtain the analytical expressions valid for $T=0$ and $|\mu|<\gamma$

$$\chi'_{j\rm A}(\omega)=A\left\{\ln\left[\frac{(1+u)(1-u+2w)}{(1-u)(1+u+2w)}\right]+\frac{4uw}{(1-u^2)}\right\}. \tag{6}$$

$$\chi''_{j\rm A}(\omega)=\pi A[\theta(|u|-1)\theta(1-|u|+2w)+2w\delta(|u|-1)], \tag{7}$$

where $A=ge\gamma/4\pi\hbar v$, $u=\hbar\omega/\gamma$, and $w=|\mu|/\gamma$. Similar analytical expressions can be obtained for $\mu>\gamma$.

To compute the optical conductivity Eq. (2) we evaluate the complex function $\chi_{j\rm A}(\omega)$ at the phonon resonance $\omega_{\rm A}\approx 0.2$ eV, using standard values for $\hbar v=6.74$ eV Å and $\gamma=0.39$ eV. From the value $\alpha=6.4$ eV Å^{-1} (Ref. 21) of the deformation potential we get $g=0.27$ eV, corresponding to the dimensionless parameter $\lambda=(\sqrt{3}/\pi)g^2/(\hbar v/a)^2=6\times10^{-3}$ (Ref. 17), in agreement with the experimental estimates given in Refs. 13 and 15. The resulting spectral weight $W_{\rm A}$ as evaluated from Eq. (2) and Eqs. (4) and (5) is shown in Fig. 2 for $\eta=0$ and $\eta=30$ meV, along with the experimental data $W_{\rm exp}$, $W'_{\rm exp}$ taken from Ref. 15. Note that the

only possible electron-hole excitations at the phonon energy $\omega_A(<\gamma)$, namely, the 2–3 multiband transitions, are not allowed in Eq. (4). Thus in the clean limit $\chi_{jA}(\omega_A)\approx 0$, so that no Fano effect ($q_A=-\infty$) is found and $W'_A=W_A$ while for $\eta \neq 0$ a small contribution to $\chi''_{jA}(\omega_A)$ from the other interband transitions gives rise to a weak Fano asymmetry, and hence $W'_A \lesssim W_A$, as shown in Fig. 2. Both the magnitude of W_A, which is proportional to the dimensionless coupling λ, and its doping dependence are in excellent agreement with W_{exp}, pointing out that the E_u mode is the main responsible for the phonon infrared intensity reported in Ref. 15 at large n. On the other hand, even in the presence of a large η, the above calculations do not account for the negative integrated weight W'_{exp} observed around $n\approx 0$ (Fig. 2), which has been attributed in Ref. 16 to the onset of the E_g mode in the presence of a finite potential asymmetry Δ. These observations suggest thus that different phonon modes can be optically relevant in different regions of the phase space.

Our theoretical framework allows us to investigate the possibility of such phonon switching by taking into account explicitly the role of Δ. When $\Delta \neq 0$ two effects must be taken into account: (i) the phonon eigenmodes of the systems do not correspond any more to E_u and E_g, even though the new phonon eigenfrequencies $\omega_\pm$ follow closely the doping dependence of the $\omega_{A,S}$ of the uncoupled modes.[22,23] As a consequence the phonon propagator D_{AA} can develop at large Δ a second peak with weaker intensity at approximately the frequency ω_S of the E_g mode. Note, however, that according to Eq. (1) the infrared activity of the D_{AA} phonon propagator is still ruled by the strength p_A. Since, as we shall see below, p_A vanishes for $n\to 0$ also when $\Delta \neq 0$, the appearance of the IR phonon structures at $n\approx 0$ (Refs. 15 and 16) cannot be accounted for by the mixing of the modes; (ii) in addition to the previous effect, the presence of a finite Δ leads also to a finite mixed response function $\chi_{jS}(\omega)=-\langle jV_S\rangle_\omega \neq 0$. Equation (1) must be thus generalized as

$$\chi^{ep}_{jj}(\omega)=\chi_{jA}(\omega)D_{AA}(\omega)\chi_{A^\dagger j}(\omega)+\chi_{jS}(\omega)D_{SS}(\omega)\chi_{S^\dagger j}(\omega) + [\chi_{jA}(\omega)D_{AS}(\omega)\chi_{S^\dagger j}(\omega)+\text{H.c.}], \quad (8)$$

where $\chi_{S^\dagger j}(\omega)=\chi_{jS}(\omega)$ and $D_{\nu\nu'}(\omega)=-\langle\phi_\nu\phi_{\nu'}\rangle_\omega$ are the phonon propagators, calculated including the hybridized phonon self-energy χ_{AS} for finite Δ.[22,23] Equation (8) shows how, due to the χ_{jS} response triggered by the finite Δ, a *direct* coupling channel to the symmetric E_g mode vibrations (the D_{SS} phonon propagator) appears in the optical spectroscopy. Similar expressions as Eqs. (4) and (5) can be derived for χ_{jS}, where, however, the coefficients $C^{nm}_{jS,\mathbf{k}}$, as well as $C^{nm}_{jA,\mathbf{k}}$, have a more complex structure for $\Delta \neq 0$.

To elucidate the competition between the different optical channels in Eq. (8) we compute explicitly χ_{jA} and χ_{jS} for generic Δ and μ, giving a complete phase diagram that can be explored in double-gated samples. To parameterize the strengths of the relative channels we use the quantities $p_\nu=\pi|\chi_{j\nu}|^2/\omega_{av}$ for $\nu=A,S$ and $p_{AS}=\pi|\chi_{jA}\chi_{jS}|/\omega_{av}$ for the mixed channel, where ω_{av} is the average frequency of the two poles of the phonon propagators.[22,23] For a direct comparison with experimental data, we set $T=10$ K and $\eta=30$ meV, which is halfway between $\eta=18$ meV reported in Ref. 7 and $\eta=40$ meV in Ref. 16. The results for the phonon strengths and Fano factors are plotted as a color map in the Δ-μ space in Figs. 3(a)–3(f) where also the Δ-μ location of the available IR data[15,16] is shown.

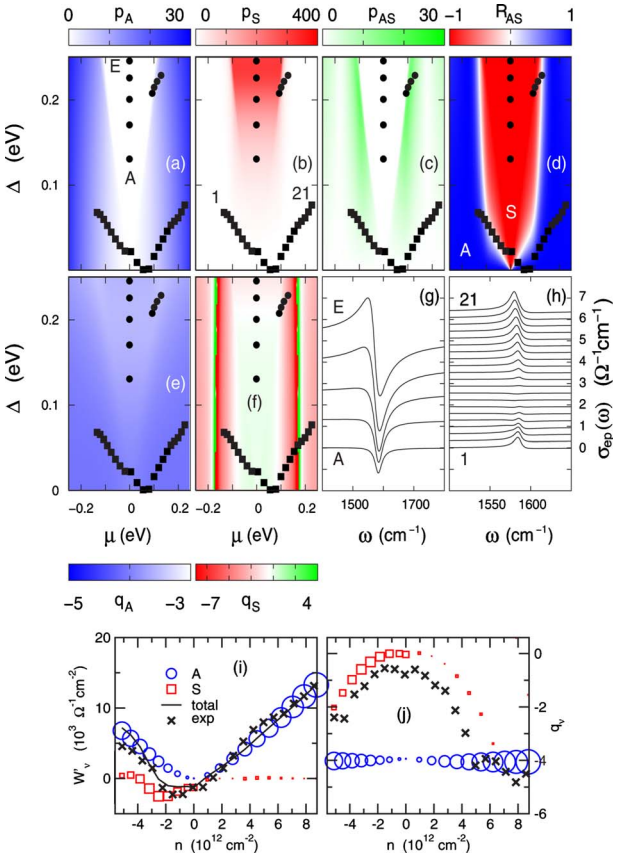

FIG. 3. (Color online) (a)–(c) Strength p_ν of the different electron-phonon contributions to the optical conductivity. The above color scale is in units of 10^3 Ω^{-1} cm^{-2}. (d) Relative phonon weight R_{AS}. (e)–(f) Fano-asymmetry factors q_A and q_S. Also shown in these plots is the Δ-μ location of experimental data: (Ref. 16) (●) and (Ref. 15) (■). The corresponding optical spectra are shown in panels (g) ($\mu=0$ and increasing Δ from A to E) and (h) (increasing doping from 1 to 21), respectively. Curves are displaced vertically for clarity. (i) Different electron-phonon contributions W'_ν (open symbols) to total ω-integrated spectral weight (solid line) calculated for Δ-μ of Ref. 15. (j) corresponding Fano factors q_ν from Eq. (3). The size of the open symbols in panels (i) and (j) is proportional to p_ν. Crosses are experimental data from Ref. 15.

Figures 3(a) and 3(b) show that the main parameter tuning the strength of the E_u mode is the charge doping whereas the E_g mode is active mainly around the neutrality point with a strength that is tuned by the asymmetry gap Δ. The strength of the mixed optical structure [third line in Eq. (8)], shown in Fig. 3(c), satisfies $p_{AS}\ll p_A, p_S$ in a large part of the phase diagram so that only A and S channels [first two lines in Eq. (8)] are active. The relative intensity $R_{AS}=(p_A-p_S)/(p_A+p_S)$ is summarized in Fig. 3(d), where $R_{AS}\approx 1$ corresponds a dominant E_u mode while $R_{AS}\approx -1$ gives a dominant E_g resonance. Note that the region $R_{AS}\approx 0$ where the two strengths of the optical structures have similar magnitude is quite narrow and difficult to resolve experimentally. In Figs.

3(e) and 3(f), we plot also the relative Fano factor q_ν for A and S modes. As one can see, q_A is essentially doping independent while q_S shows a sizeable dependence as function of μ. These behaviors can be understood considering that the structure of Eq. (4) for χ_{jA} is still valid for $\Delta \neq 0$, so that the low-energy 2–3 interband transitions are missing and the weak Fano asymmetry of the A mode is only due to a finite broadening due to η on the remaining transitions. On the contrary *all* the interband transitions contribute to χ_{jS}, including, in particular, the low-energy 2–3 interband transitions which overlap with the phonon frequency (for $2|\mu| \leq \omega_S$), accounting for the sizable dependence of q_S as function of μ.

The comparison of the present results with the Δ-μ location of the experimental available data provides an important route to check our theoretical predictions. In Figs. 3(g) and 3(h) we show the optical conductivity $\sigma'_{ep}(\omega)$ using Eq. (8) for the μ,Δ values corresponding to the experimental data of Refs. 15 and 16. The phonon propagators $D_{\nu\nu'}$ are computed taking account the self-energy hybridization due to $\Delta \neq 0$,[22,23] and convoluted with the experimental resolution of 10 cm^{-1}.[15] In Fig. 3(g) we plot the spectra for $\mu=0$, showing the evolution of the optical intensity and of the Fano asymmetry for increasing Δ. These features are related uniquely to the E_g S mode,[16] consistently with panels (a) and (b). On the contrary the spectra in Fig. 3(h), evaluated at the doping levels and electrostatic potentials of Ref. 15, are expected to show a continuous switching between A and S modes, depending on the values of μ and Δ. To investigate deeper this issue, we plot in Fig. 3(i) the theoretical spectral weights W'_ν for both E_u and E_g modes evaluated on the set of experimental data Δ-μ of Ref. 15. The size of the symbols is proportional to the peak strength p_ν. The switch between the E_u phonon peak and the E_u one in the regime $n \in [-1:3] \times 10^{12}$ cm^{-2} is evident and is reflected in a total spectral weight $W'_T = W'_A + W'_S$ which becomes negative in such n region, in good agreement with the experimental ω-integrated weight W'_{exp}. A similar phonon switch is also evident from the analysis of the Fano asymmetry, reported in Fig. 3(j). Also here one can distinguish the crossover between a constant q behavior at large n, which we can attribute to the E_u mode, and a drop of $|q|$ at small n in the region where the E_g mode becomes dominant. The experimental fit, done with a single-mode Fano formula, presents a similar trend.

We stress that the switching between E_u and E_g modes in the optical conductivity discussed here is not related to the possible appearance at large Δ of a double-peak structure in each of D_{AA} or D_{SS} propagators.[13,14,22,23] Even though the two effects could be present simultaneously at large gap values, the optical data available so far are outside the region where the two peaks can be resolved.

In conclusion, in this Rapid Communication we presented a complete theoretical description of the phonon resonance in bilayer graphene that accounts for both the intensity and the Fano-asymmetry variations as functions of the density and the gap. We also showed that an optical switching from E_u to E_g can be induced in a controlled way, providing a full understanding of the experimental data.

The derived phase diagram for the optical properties offers a roadmap for the characterization of graphenic systems. For instance, the measurement of the IR intensity of the phonon peak can provide a useful tool to determine the doping level in contact-free samples.

We thank A. V. Balatsky, F. Bernardini, F. Mauri, and P. Postorino for enlightening discussions. This work was supported by the Swiss National Science Foundation (SNSF) under the Grant No. 200021-120347 and under MaNEP, and by Italian MIUR project PRIN 2007FW3MJX.

[1] E. McCann, Phys. Rev. B **74**, 161403(R) (2006).
[2] E. V. Castro, K. S. Novoselov, S. V. Morozov, N. M. R. Peres, J. M. B. Lopes dos Santos, J. Nilsson, F. Guinea, A. K. Geim, and A. H. Castro Neto, Phys. Rev. Lett. **99**, 216802 (2007).
[3] J. B. Oostinga *et al.*, Nature Mater. **7**, 151 (2008).
[4] Y. Zhang *et al.*, Nature (London) **459**, 820 (2009).
[5] K. F. Mak, C. H. Lui, J. Shan, and T. F. Heinz, Phys. Rev. Lett. **102**, 256405 (2009).
[6] A. B. Kuzmenko, E. van Heumen, D. van der Marel, P. Lerch, P. Blake, K. S. Novoselov, and A. K. Geim, Phys. Rev. B **79**, 115441 (2009).
[7] A. B. Kuzmenko, I. Crassee, D. van der Marel, P. Blake, and K. S. Novoselov, Phys. Rev. B **80**, 165406 (2009).
[8] C. Stampfer *et al.*, Appl. Phys. Lett. **91**, 241907 (2007).
[9] A. C. Ferrari *et al.*, Phys. Rev. Lett. **97**, 187401 (2006).
[10] J. Yan, Y. Zhang, P. Kim, and A. Pinczuk, Phys. Rev. Lett. **98**, 166802 (2007).
[11] S. Pisana *et al.*, Nature Mater. **6**, 198 (2007).
[12] J. Yan, E. A. Henriksen, P. Kim, and A. Pinczuk, Phys. Rev. Lett. **101**, 136804 (2008).
[13] L. M. Malard, D. C. Elias, E. S. Alves, and M. A. Pimenta, Phys. Rev. Lett. **101**, 257401 (2008).
[14] J. Yan, T. Villarson, E. A. Henriksen, P. Kim, and A. Pinczuk, Phys. Rev. B **80**, 241417(R) (2009).
[15] A. B. Kuzmenko, L. Benfatto, E. Cappelluti, I. Crassee, D. van der Marel, P. Blake, K. S. Novoselov, and A. K. Geim, Phys. Rev. Lett. **103**, 116804 (2009).
[16] T.-Ta Tang *et al.*, Nat. Nanotechnol. **5**, 32 (2010).
[17] T. Ando, J. Phys. Soc. Jpn. **76**, 104711 (2007).
[18] M. J. Rice, Phys. Rev. Lett. **37**, 36 (1976); M. J. Rice and H.-Y. Choi, Phys. Rev. B **45**, 10173 (1992).
[19] E. J. Nicol and J. P. Carbotte, Phys. Rev. B **77**, 155409 (2008).
[20] U. Fano, Phys. Rev. **124**, 1866 (1961).
[21] A. H. Castro Neto and F. Guinea, Phys. Rev. B **75**, 045404 (2007).
[22] T. Ando and M. Koshino, J. Phys. Soc. Jpn. **78**, 034709 (2009).
[23] P. Gava, M. Lazzeri, A. M. Saitta, and F. Mauri, Phys. Rev. B **80**, 155422 (2009).